A low temperature investigation of the gas-phase N(2 D) + NO reaction. Towards a viable source of N(2 D) atoms for kinetic studies in astrochemistry

Dianailys Nuñez-Reyes, Kevin Hickson

A Low Temperature Investigation of the Gas-Phase $N(^2D) + NO$ Reaction. Towards a Viable Source of $N(^2D)$ Atoms for Kinetic Studies in Astrochemistry

Dianailys Nuñez-Reyes[a,b] and Kevin M. Hickson,*[,a,b]

[a]*Université de Bordeaux, Institut des Sciences Moléculaires, F-33400 Talence, France*

[b]*CNRS, Institut des Sciences Moléculaires, F-33400 Talence, France*

Abstract

The gas-phase reaction of metastable atomic nitrogen $N(^2D)$ with nitric oxide has been investigated over the 296 - 50 K temperature range using a supersonic flow reactor. As $N(^2D)$ could not be produced photolytically in the present work, these excited state atoms were generated instead through the $C(^3P) + NO \rightarrow N(^2D) + CO$ reaction while $C(^3P)$ atoms were created in-situ by the 266 nm pulsed laser photolysis of CBr_4 precursor molecules. The kinetics of $N(^2D)$ atoms were followed on-resonance by vacuum ultraviolet laser induced fluorescence at 116.7 nm. The measured rate constants for the $N(^2D) + NO$ reaction are in excellent agreement with most of the earlier work at room temperature and represent the only available kinetic data for this process below 296 K. The rate constants are seen to increase slightly as the temperature falls to 100 K with a more substantial increase at even lower temperature; a finding which is not reproduced by theoretical work. The prospects for using this chemical source of $N(^2D)$ atoms in future studies of a wide range of $N(^2D)$ atom reactions are discussed.

Introduction

Excited state metastable nitrogen atoms N(^{2}D) are thought to play important roles in the chemistry of a range of planetary atmospheres. In the terrestrial upper atmosphere these atoms are produced by various processes including the dissociative excitation of N_2 by energetic electrons and by short wavelength N_2 photolysis[1]. The reaction between N(^{2}D) with atmospheric O_2 is considered to be a major source of both NO and metastable O(^{1}D) atoms[2] in the Earth's lower thermosphere around 110 km, while the reaction between N(^{2}D) and NO limits the total concentration of N(^{2}D) at these altitudes. As N_2 is an important component of the atmospheres of Mars and Titan, the reactions of N(^{2}D) are also important processes in the photochemistry of both these planets. Indeed, N(^{2}D) reacts rapidly with CO_2 in the Martian atmosphere to form NO and CO[3] whereas the reactions between N(^{2}D) and the various saturated and unsaturated hydrocarbons present in the atmosphere of Titan are considered to be major sources of N-bearing organic molecules[4-6]. From an experimental point of view, there are several major difficulties associated with the investigation of the kinetics of N(^{2}D) reactions. Firstly, convenient photolytic sources of N(^{2}D) atoms are very rare, usually requiring radiation in the vacuum ultraviolet (VUV) wavelength range to dissociate nitrogen containing precursor molecules. Husain et al.[7, 8] employed the flash photolysis of N_2O at wavelengths greater than 105 nm in their experiments whereas Umemoto et al.[9] used the multiphoton dissociation of NO molecules with photons around 275.3 nm as the source of N(^{2}D) in their experiments. On the detection side, the radiative transition from the ^{2}D state to the ground ^{4}S state is too weak to produce measureable emission in the visible region[10] so that other methods are generally employed to follow the progress of N(^{2}D) reactions such as electron spin resonance[11, 12], mass spectroscopy[13] and resonance absorption[7, 14] and emission spectroscopy[15, 16]. More recently, Umemoto et al.[17] detected N(^{2}D) atoms by the 269 nm two-photon excitation of N atoms

through the $2p^3\ ^2D_{5/2}$ - $2p^23p\ ^2S$ transition. Rapid relaxation to the $2p^23s\ ^2P$ state followed by VUV fluorescence at 149 nm allowed these authors to determine rate constants for various $N(^2D)$ reactions at room temperature. One system that has received considerable experimental and theoretical attention in the past is the reaction between $N(^2D)$ and NO

$$N(^2D) + NO \rightarrow N_2 + O(^3P, ^1D, ^1S) \qquad (1)$$

On the experimental side, earlier measurements at room temperature[7, 8, 15, 17-19] have determined rate constants for this process in the range $(0.35 - 1.8) \times 10^{-10}$ $cm^3\ s^{-1}$ with a recommended value of $k_{N(^2D)+NO}(298\ K) = 6 \times 10^{-11}$ $cm^3\ s^{-1}$ [20]. The equivalent reaction of ground state atomic reaction $N(^4S)$ is thought to be slower at room temperature and below[21]. To the best of our knowledge, no previous experimental studies of reaction (1) have been performed at other temperatures. On the theoretical side, Gonzalez et al.[22] investigated the channel leading to N_2 and $O(^1D)$ as products, through ab initio CASSCF/CASPT2 electronic structure calculations of the ground $^1A'$ potential energy surface coupled with quasiclassical trajectory (QCT) calculations to obtain the rate constant over the temperature range 300 - 1500 K. They identified several different reactive mechanisms including attack by the $N(^2D)$ atom on both the O-atom and N-atom ends of the NO molecule to form products N_2 and $O(^1D)$ over the barrierless $^1A'$ surface. They obtained a rate constant value for this channel of $(2.63 \pm 0.04) \times 10^{-12}$ $cm^3\ s^{-1}$, more than an order of magnitude lower than the lowest experimental value for the total rate constant at room temperature. More recently, Li et al.[23] performed QCT calculations over the 5 - 3000 K range using a double many-body expansion potential energy surface for ground state $N_2O(^1A')$ with an accurate description of the long-range interactions[24]. The derived rate constants were seen to be larger than those obtained by Gonzalez et al., with $k_{N(^2D)+NO\rightarrow O(^1D)+N_2}(300\ K) = (2.03 \pm 0.01) \times 10^{-11}$ $cm^3\ s^{-1}$. The rate constant was found to decrease with temperature, in contrast with the work by Gonzalez et al.[22] who determined the opposite temperature dependence.

Here we report the first measurements of the total rate constant for the $N(^2D)$ + NO reaction over the 50 - 296 K range using a continuous supersonic flow reactor. In the absence of efficient photolytic schemes for $N(^2D)$ production in accessible wavelength ranges, these atoms were generated instead by chemical reaction. $N(^2D)$ atoms were detected directly by pulsed laser induced fluorescence in the vacuum ultraviolet wavelength range. The methods used in this investigation are described in Section 2. Section 3 presents the data analysis methodology and the results obtained. The conclusions are outlined in Section 4.

2 Experimental

A continuous supersonic flow (Laval nozzle) reactor[25] was used in the present investigation. Detailed descriptions of the main features of the apparatus have been provided in earlier work[26, 27] with other modifications specifically related to the efficient generation of short wavelength tunable VUV radiation for the detection of atomic species reported in later studies[28-31]. In contrast to earlier studies of the reactions of $O(^1D)$ and $C(^1D)$ atoms, it was possible to use both Ar- and N_2-based Laval nozzles in this study, given the slow rate constants for the $N(^2D) + N_2$[32] and $N(^2D)$ + Ar[19] quenching reactions. The calculated and measured properties of the Laval nozzles used during this work are listed in Table 1.

Table 1 Characteristics of the supersonic flows

Mach number	1.83± 0.02[a]	1.99 ± 0.03	2.97 ± 0.06	3.85 ± 0.05
Carrier gas	N_2	Ar	Ar	Ar
Density ($\times 10^{16}$ cm^{-3})	9.4 ± 0.2	12.6 ± 0.3	14.7 ± 0.6	25.9 ± 0.9
Impact pressure (Torr)	8.2 ± 0.1	10.5 ± 0.2	15.3 ± 0.5	29.6 ± 1.0
Stagnation pressure (Torr)	10.3	13.9	34.9	113
Temperature (K)	177 ± 2	127 ± 2	75 ± 2	50 ± 1
Mean flow velocity (ms^{-1})	496 ± 4	419 ± 3	479 ± 3	505 ± 1
Chamber pressure (Torr)	1.4	1.5	1.2	1.4

[a] The errors on the Mach number, density, temperature and mean flow velocity (1σ) are calculated from separate measurements of the impact pressure using a Pitot tube as a function of distance from the Laval nozzle and the stagnation pressure within the reservoir.

In addition, measurements were also performed at room temperature (without a Laval nozzle) through a procedure which used lower flow velocities. In these types of experiments, the minor reagent radical species are normally produced in-situ within the supersonic flow through the photolysis of suitable precursor molecules. The photolysis laser is aligned along the axis of the flow to create a column of radicals with uniform density along the entire length of the flow (assuming only weak absorption along the length of the flow). In the case of $N(^2D)$ atoms however, there are no known precursor molecules in the UV wavelength range, except through multiphoton processes. In this way, Umemoto et al.[17] produced $N(^2D)$ atoms in their kinetic experiments through the multiphoton dissociation of NO, by focusing a tuneable laser at 275.3 nm into their reactor. Unfortunately, this technique cannot be applied in the present experiments given the requirement to produce a uniform density of radicals along the length of the flow. Instead, $N(^2D)$ atoms were generated here through the reaction of ground state carbon atoms $C(^3P)$ with NO molecules

$$C(^3P) + NO \rightarrow N(^2D, {}^4S) + CO \quad (2a)$$

$$\rightarrow O(^3P) + CN \quad (2b)$$

where the branching ratio $[N(^2D) + N(^4S)]/[O(^3P)]$ has previously been estimated to be 1.5 ± 0.3 at room temperature[33] with a total rate constant $k_{C(^3P)+NO}(298\ K) = 1.5 \times 10^{-10}$ cm^3 s^{-1} increasing to slightly to 2.0×10^{-10} cm^3 s^{-1} at 50 K.[34] According to previous theoretical work, channel (2a) is expected to decrease as the temperature falls.[35] $C(^3P)$ atoms were created by the 10 Hz pulsed sequential multiphoton dissociation of carbon tetrabromide,[36] CBr_4, at 266 nm with pulse energies around 24 mJ. In this case, the photolysis laser was unfocused. CBr_4 molecules were introduced into the reactor by flowing a small fraction of the carrier gas (Ar or

N_2) over solid CBr_4 held in a separate flask at a fixed temperature of 298 K. Gas-phase concentrations of CBr_4 were lower than 3.2×10^{13} cm^{-3} in the supersonic flow, as estimated using the saturated CBr_4 vapour pressure at room temperature. Previous work performed under similar conditions[28] showed that the major photolysis product is $C(^3P)$, with a small non-negligible production of $C(^1D)$ atoms. Although $C(^1D)$ atoms also react with NO molecules with rate constants which are smaller than those of the equivalent ground state carbon reaction,[37] the products are likely to be similar to those of the $C(^3P)$ + NO reaction, with the added possibility of $O(^1D)$ formation. Among the potential reaction products, only secondary reactions of CN radicals and $O(^1D)$ atoms could potentially interfere with our kinetic study of the $N(^2D)$ + NO reaction (the $O(^3P)$ + NO association reaction is slow[38]). The CN + NO reaction is thought to proceed mostly by association at low temperature,[39] so this secondary process is also unlikely to interfere with the present measurements. Moreover, the only exothermically available products of the $O(^1D)$ + NO reaction are $N(^4S) + O_2$, which are only accessible through nonadiabatic transitions.[40] Neither of these products should influence the $N(^2D)$ kinetics measurements.

$N(^2D)$ atoms were detected directly in the present experiments by on-resonance pulsed laser induced fluorescence in the vacuum ultraviolet wavelength range (VUV LIF) through the $2s^22p^3\ ^2D^\circ$ - $2s^22p^2(^3P)3d\ ^2F$ transition at 116.745 nm. To obtain tunable light at this wavelength, the 700.5 nm output of a pulsed tunable dye laser was first injected into a BBO crystal, allowing radiation around 350.25 nm to be generated by second harmonic generation with a pulse energy of approximately 8 mJ. After separation of the fundamental radiation, the UV beam was steered and focused into a cell containing 40 Torr of Xe and 560 Torr of Ar for phase matching purposes, generating tunable VUV radiation by frequency tripling. The cell itself was attached to a 75 cm long side arm positioned at right angles to the reactor at the level of the detection region. The side arm was constantly flushed by either Ar or N_2 to avoid

attenuation of the VUV beam by reactive gases in the chamber. A MgF_2 lens at the exit of the cell allowed the VUV beam to be collimated while most of the divergent residual UV radiation was trapped by circular baffles placed along the length of the sidearm. VUV emission from excited N(^{2}D) atoms in the cold supersonic flow was collected by a LiF lens and focused onto the photocathode of a solar blind photomultiplier tube (PMT). The PMT was protected from reactive gases in the chamber by a LiF window while the region between the PMT and the LiF window was evacuated to prevent supplementary VUV absorption losses by atmospheric O_2. The PMT output was fed into a fast preamplifier which was connected to a boxcar module for signal processing and integration. The delay time between photolysis and probe lasers was scanned by a digital delay generator. 30 laser shots were recorded at each delay time with at least 90 time points for each decay profile. Laser shots were also recorded at negative time delays to set the fluorescence signal baseline level. All gases used in the experiments were flowed from cylinders with no further purification prior to use, while the flows of the carrier gases and reactive gases were regulated by calibrated mass-flow controllers. The suppliers and purities of the gases used are listed below (Linde Ar 99.999%, Xe 99.999%, Air Liquide N_2 99.999%, NO 99.9%).

3 Results and Discussion

In order to apply the pseudo-first-order approximation, the concentration of NO was maintained in excess with respect to both C(^{3}P) and N(^{2}D) atoms in these experiments. The variation of the N(^{2}D) VUV LIF signal as a function of time is displayed in Figure 1 for two different values of [NO] recorded at 50 K.

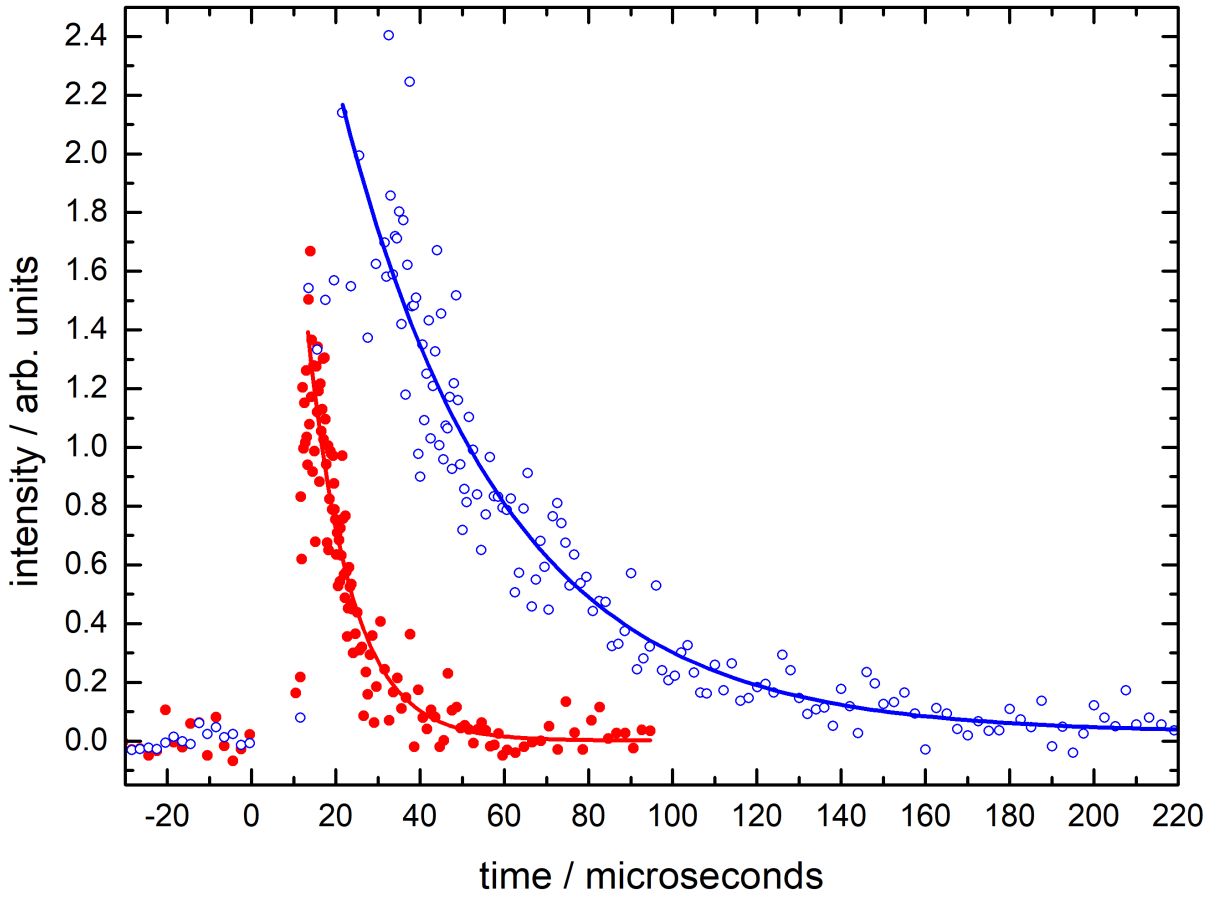

Figure 1 N(^{2}D) VUV LIF signal as a function of time recorded at 50 K. (Red solid circles) [NO] = 8.3 × 10^{14} cm^{-3}; (blue open circles) [NO] = 1.6 × 10^{14} cm^{-3}. Solid red and blue lines represent exponential fits to the data.

Under these conditions, as N(^{2}D) atoms are formed by reaction (2a) and consumed by reaction (1), the N(^{2}D) VUV LIF signal should take the form of a biexponential function

$$I_{N(^2D)} = A(\exp(-k'_a t) - \exp(-k'_b t)) \qquad (3)$$

where $I_{N(^2D)}$ is the time dependent N(^{2}D) VUV LIF signal, A is a constant, k'_a is the pseudo-first-order rate constant for N(^{2}D) loss, k'_b is the pseudo-first-order rate constant for N(^{2}D) formation and t is the time. As the N(^{2}D) VUV LIF signal levels were small compared with those recorded during our earlier studies of C(^{3}P), O(^{1}D) and H(^{2}S) reaction kinetics, it was necessary to amplify the PMT output signal using a fast preamplifier. Although the PMT was

supposed to be insensitive to radiation in the UV range, with an expected cutoff around 200 nm, scattered light (and/or window fluorescence) generated by the photolysis laser lead to saturation of the PMT for the first 15 microseconds after the photolysis laser pulse. Consequently, the expected rise of the N(^{2}D) VUV LIF signal could not be recorded close to zero. Instead, a single exponential decay function of the form

$$I_{\mathrm{N}(^2\mathrm{D})} = \mathrm{A}\exp(-k'_{\mathrm{a}}t) \qquad (4)$$

was used to fit the N(^{2}D) VUV LIF signals as shown in Figure 1. Here, $k'_{\mathrm{a}} = k_{\mathrm{N}(^2\mathrm{D})+\mathrm{NO}}[\mathrm{NO}] + k_{\mathrm{N}(^2\mathrm{D})+\mathrm{X}}[\mathrm{X}] + k_{\mathrm{diff,N}(^2\mathrm{D})}$ where $k_{\mathrm{N}(^2\mathrm{D})+\mathrm{NO}}$ is the second-order rate constant for reaction (1), $k_{\mathrm{N}(^2\mathrm{D})+\mathrm{X}}[\mathrm{X}]$ is a term corresponding to other first-order reactive losses of N(^{2}D) atoms (such as through the N(^{2}D) + CBr_4 reaction for example) and $k_{\mathrm{diff,N}(^2\mathrm{D})}$ represents the first-order diffusional loss of N(^{2}D) atoms. In this instance, the starting point for the fits had to be chosen carefully to avoid fitting to the rising part of the temporal profiles. In practice, this was achieved relatively easily by displaying the N(^{2}D) VUV LIF signals on a logarithmic scale and by carefully selecting the 'linear' part of the decay curves. Fortunately, as the rate constant for reaction (2) is thought to be somewhat larger than the rate constant for reaction (1) (at least at room temperature[20, 34]), simulations indicated that N(^{2}D) formation was complete (assuming a delay corresponding to four half-lives had elapsed) for all but a few kinetic profiles within the first 100 microseconds after C(^{3}P) formation.

Decays similar to those shown in Figure 1 were recorded for a range of [NO], allowing a wide range of k'_a values to be derived. Plots of k'_a as a function of the corresponding [NO] at any given temperature allowed the second-order rate constant to be determined through weighted linear least-squares fits to the datapoints. Figure 2 shows examples of these second-order plots obtained at 296 K, 75 K and 50 K.

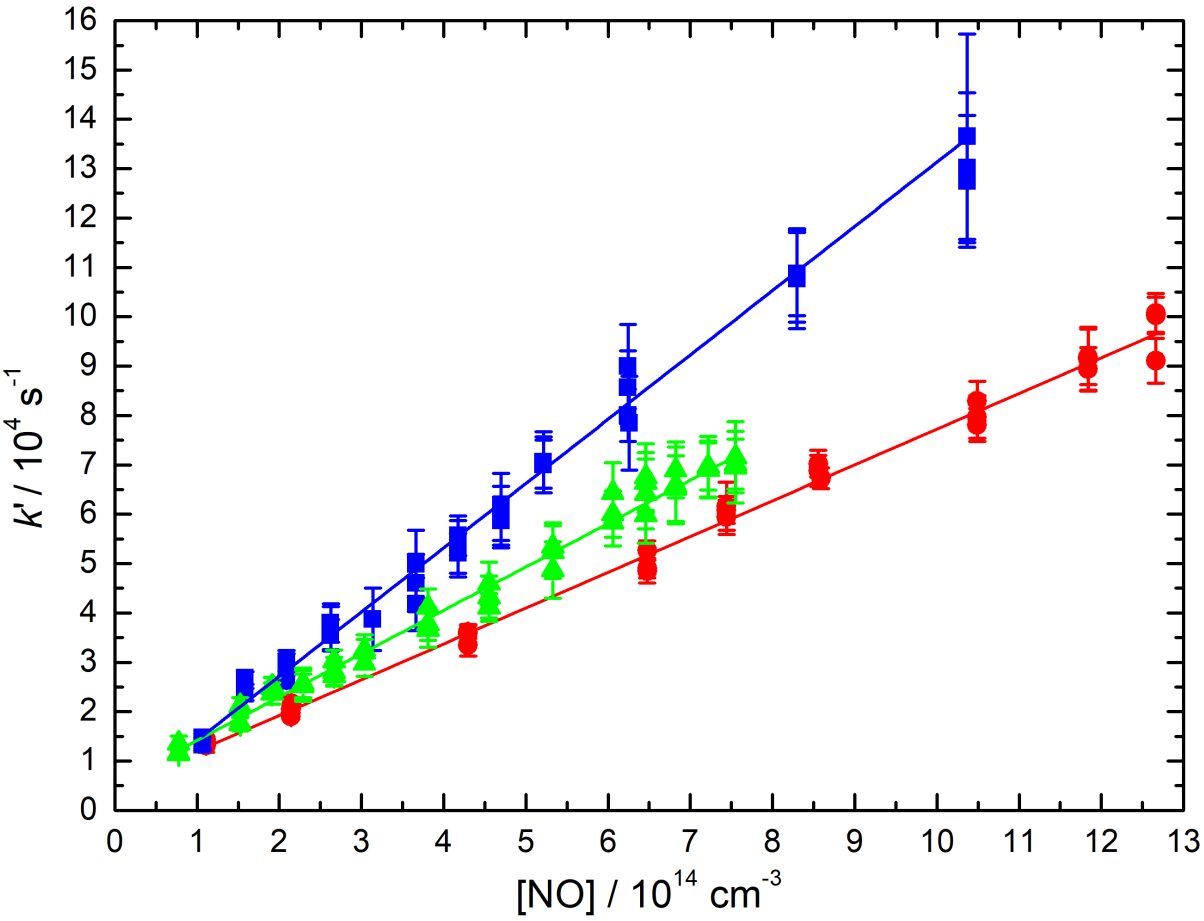

Figure 2 Second-order plots for the N(^{2}D) + NO reaction. (Red solid circles) data recorded at 296 K; (green solid triangles) data recorded at 75 K (blue solid squares) data recorded at 50 K. The solid red, green and blue lines represent linear least-squares fits to the datasets, weighted by the statistical uncertainties of the individual datapoints (obtained through single exponential fits of expression (4) to curves similar to those shown in Figure 1).

The second-order rate constants are displayed as a function of temperature in Figure 3 alongside earlier experimental and theoretical work.

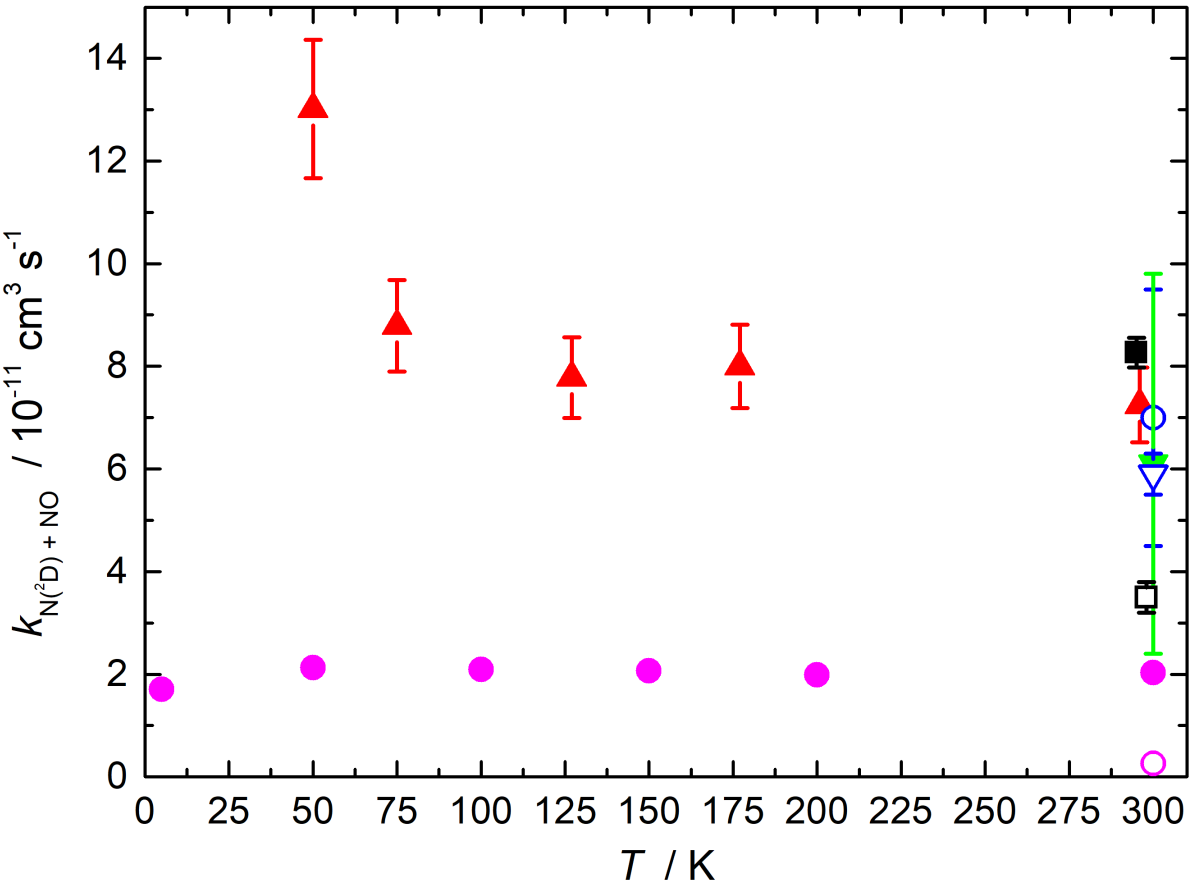

Figure 3 Rate constants for the N(^{2}D) + NO reaction as a function of temperature. Experimental studies (solid red triangles) this work; (open blue circles) Lin and Kaufmann[19]; (black solid square) Umemoto et al.[17]; (black open square) Sugawara et al.[15]; (open blue triangle) Husain et al.[8]; (solid green triangle) Husain et al.[7]. Theoretical studies (open purple circle) Gonzalez et al.[22]; (solid purple circles) Li et al. [23] Error bars on the present results represent the combined statistical (1σ) and systematic (10 %) uncertainties.

These values are also summarized in Table 2 alongside other information such as the number of measurements and the range of [NO] used.

Table 2 Temperature dependent rate constants for the N(^{2}D) + NO reaction

T / K	N^b	[NO]/ 10^{14} cm^{-3}	$k_{N(^2D)+NO}$ / cm^3 s^{-1}

296	29	1.11-12.66	$(7.25 \pm 0.73)^{c} \times 10^{-11}$
177 ± 2 [a]	36	0.72-8.06	$(8.00 \pm 0.81) \times 10^{-11}$
127 ± 2	28	0.81-9.16	$(7.78 \pm 0.79) \times 10^{-11}$
75 ± 2	43	0.78-7.55	$(8.79 \pm 0.89) \times 10^{-11}$
50 ± 1	35	1.07-10.37	$(13.02 \pm 1.35) \times 10^{-11}$

[a]Uncertainties on the calculated temperatures represent the statistical (1σ) errors obtained from Pitot tube measurements of the impact pressure. [b]Number of individual measurements. [c]Uncertainties on the measured rate constants represent the combined statistical (1σ) and estimated systematic (10%) errors.

Both statistical and systematic uncertainties contribute to the error limits on these values. Statistical errors were obtained through the weighted linear-least squares fitting procedure used to derive second-order rate constants (see Figure 2). An estimated systematic error of 10% was also included, a value which was chosen to account for the possible contributions of errors in the calibration of the mass-flow controllers and the subsequent determinations of the concentrations of the reactants and the supersonic flow density as well as possible errors in pressure gauges and other instruments.

On the experimental side, the measured rate constant at 296 K, $k_{\mathrm{N(^2D)+NO}}(296\ \mathrm{K}) = (7.3 \pm 0.7) \times 10^{-11}$ cm^3 s^{-1} is in good agreement with all but two of the previous determinations of the rate constant at room temperature,[7, 8,17,19] with values in the range $(5.9\text{-}8.3) \times 10^{-11}$ cm^3 s^{-1} using a variety of methods to follow the progress of the reaction. Indeed, this good agreement with the majority of earlier studies goes a long way to validating the novel strategy for N(^{2}D) production developed in the present investigation. The measurements by Black et al.[18] and Sugawara et al.[15] of $k_{\mathrm{N(^2D)+NO}}(298\ \mathrm{K}) = (1.8 \pm 0.5) \times 10^{-10}$ cm^3 s^{-1} and $(3.5 \pm 0.3) \times 10^{-11}$ cm^3 s^{-1} derived

rate constants that are considerably higher and lower respectively than all other values and the recommended room temperature value of 6×10^{-11} cm^3 s^{-1} [20]. The low rate constant value reported by Sugawara et al.[15] has been attributed to possible errors in the determination of the NO concentration.

Below room temperature, the present study indicates that the rate constant displays a slight negative temperature dependence over the 296 K - 75 K range followed by a more marked increase at even lower temperature, reaching a value of $(1.3 \pm 0.1) \times 10^{-10}$ cm^3 s^{-1} at 50 K.

On the theoretical side, it can be seen from Figure 3 that the QCT study of the $N(^2D)$ + NO reaction by Gonzalez et al.[22] predicts a rate constant that is more than an order of magnitude smaller than all the experimental values at room temperature. This work was based on the ground singlet 1 $^1A'$ potential energy surface of N_2O alone, whereas there are in fact five potential energy surfaces which adiabatically correlate with $O(^1D)$ + N_2 products. In order to rationalize their results, Gonzalez et al.[22] attempted to consider the possible involvement of the other four excited potential energy surfaces. They concluded that the 2 $^1A'$ and 1 $^1A''$ surfaces might also contribute to the reactivity which could increase the rate constant to 7.9×10^{-12} cm^3 s^{-1} assuming similar values of the rate constant for these two surfaces. As further contributions to the overall rate constant are also expected from the channels leading to $O(^3P)$ + N_2 and $O(^1S)$ + N_2 as products, Gonzalez et al.[22] stated that inclusion of these other channels should lead to even better agreement between the experimental and theoretical rate constants. The more recent theoretical investigation by Li et al.[23] based on a new ground state $^1A'$ potential energy surface is seen to be in better agreement with the measured values. As N_2O intermediate formation follows a capture-type mechanism, with the dominant contribution being the electrostatic interactions between the $N(^2D)$ quadrupole and the NO dipole in addition to the $N(^2D)$ quadrupole and the NO quadrupole, Li et al.[23] attributed the improvement over the calculations of Gonzalez et al.[22] as being due to an improved description of the long-range forces.

Nevertheless, the calculated rate constants of Li et al.[23] are still four times smaller than those obtained during the present investigation, a discrepancy that almost certainly indicates the role of other channels leading to $O(^1D) + N_2$, $O(^3P) + N_2$ and $O(^1S) + N_2$ in the overall reactivity. Interestingly, the larger measured increase in reactivity below 75 K determined in the present work could be indicative of the increased contribution of another mechanism at low temperature. Indeed, Gonzalez et al.[22] hint at the possible existence of crossing seams between the lowest singlet and triplet adiabatic potential energy surfaces which might become more important as the intermediate N_2O lifetime increases.

Although the $N(^2D)$ + NO reaction itself has little or no known application in planetary atmospheres at the present time (other than the Earth's atmosphere), this study could represent an important breakthrough in the investigation of other more important reactions for planetary atmospheres due to its potential as a source of $N(^2D)$ atoms. Although the production of $N(^2D)$ atoms through reaction (2a) and their subsequent removal through reaction (1) are coupled processes, we can nonetheless envisage using these reactions to investigate other $N(^2D)$ reactions such as $N(^2D)$ + hydrocarbons that are considered to be major sources of N-bearing organic molecules in Titan's atmosphere. Crucially, none of the most abundant saturated hydrocarbon molecules in Titan's atmosphere (CH_4 and C_2H_6) react with ground state atomic carbon, our source for $N(^2D)$ atoms, so that the yield of $N(^2D)$ atoms will remain relatively unaffected by the addition of these molecules to the supersonic flow. If the NO concentration is maintained at a constant (small) value it should be possible to extract pseudo-first-order rate constants for the specific hydrocarbon reaction by varying its excess concentration. Here, $k'_a = k_{\mathrm{N}(^2\mathrm{D})+\mathrm{NO}}[\mathrm{NO}] + k_{\mathrm{N}(^2\mathrm{D})+\mathrm{HC}}[\mathrm{HC}] + k_{\mathrm{diff,N}(^2\mathrm{D})}$ where the term $k_{\mathrm{N}(^2\mathrm{D})+\mathrm{HC}}[\mathrm{HC}]$ is now the pseudo-first-order loss rate of $N(^2D)$ through reaction with the hydrocarbon. Consequently, a plot of the pseudo-first-order loss rate of $N(^2D)$ as a function of the corresponding [HC] should allow the second-order rate constants to be determined from the slope in an identical manner to

the usual analysis (see Figure 2). In this instance, the y-axis intercept value will correspond to the term $k_{\mathrm{N}(^2\mathrm{D})+\mathrm{NO}}[\mathrm{NO}]$ (assuming that diffusional losses are small in comparison). Preliminary measurements in our laboratory indicate that should be possible to use this procedure to study the kinetics of a wide variety of N(^{2}D) atom reactions down to low temperature if the excess reagent species does not react too rapidly with ground state atomic carbon.

4 Conclusions

Here we present an experimental investigation of the temperature dependent kinetics of the reactions of metastable nitrogen atoms in the ^{2}D state with nitric oxide. A Laval nozzle reactor was used to study this gas-phase reaction at temperatures as low as 50 K. As N(^{2}D) is very difficult to produce photolytically, a chemical source of these atoms was used in the present work, involving the generation of C(^{3}P) atoms through the multiphoton dissociation of CBr_4 molecules at 266 nm followed by their reaction with NO. N(^{2}D) atoms were detected directly through vacuum ultraviolet laser induced fluorescence. The derived rate constants are seen to be in excellent agreement with most of the previous studies at room temperature. Below room temperature the rate constant displays a slight negative temperature dependence down to 75 K, with a more pronounced increase at lower temperature. This work demonstrates the potential importance of this chemical source of N(^{2}D) atoms for future investigations of astrochemically relevant N(^{2}D) reactions such as those with saturated hydrocarbons.

Acknowledgements

K.M.H. and D.N.R acknowledge support from the French program ‘‘Physique et Chimie du Milieu Interstellaire” (PCMI) of the CNRS/INSU with the INC/INP co-funded by the CEA and CNES as well as funding from the "Program National de Planétologie" (PNP) of the CNRS/INSU.

References

1. J.-C. Gérard, *Planet. Space Sci.*, 1992, **40**, 337-353.
2. D. W. Rusch, J. C. Gerard and W. E. Sharp, *Geophys. Res. Lett;*, 1978, **5**, 1043-1046.
3. V. A. Krasnopolsky, *Icarus*, 1993, **101**, 313-332.
4. M. Dobrijevic, E. Hébrard, J. C. Loison and K. M. Hickson, *Icarus*, 2014, **228**, 324-346.
5. E. Hébrard, M. Dobrijevic, J. C. Loison, A. Bergeat and K. M. Hickson, *Astron. Astrophys.*, 2012, **541**, A21.
6. J. C. Loison, E. Hébrard, M. Dobrijevic, K. M. Hickson, F. Caralp, V. Hue, G. Gronoff, O. Venot and Y. Bénilan, *Icarus*, 2015, **247**, 218-247.
7. D. Husain, L. J. Kirsch and J. R. Wiesenfeld, *Faraday Discuss.*, 1972, **53**, 201-210.
8. D. Husain, S. K. Mitra and A. N. Young, *J. Chem. Soc., Faraday Trans. II*, 1974, **70**, 1721-1731.
9. H. Umemoto and K. Matsumoto, *J. Chem. Soc., Faraday Trans.*, 1996, **92**, 1315-1318.
10. Y. Ralchenko, A. E. Kramida and J. Reader, *NIST Atomic Spectra Database (ver. 4.0.1).* http://physics.nist.gov/asd. *National Institute of Standards and Technology, Gaithersburg, MD.*, 2006.
11. K. M. Evenson and H. E. Radford, *Phys. Rev. Lett.*, 1965, **15**, 916-917.
12. B. Fell, I. V. Rivas and D. L. McFadden, *J. Phys. Chem*, 1981, **85**, 224-228.
13. S. N. Foner and R. L. Hudson, *J. Chem. Phys.*, 1962, **37**, 1662-1667.
14. T. Takayanagi, Y. Kurosaki, K. Misawa, M. Sugiura, Y. Kobayashi, K. Sato and S. Tsunashima, *J. Phys. Chem. A*, 1998, **102**, 6251-6258.
15. K. Sugawara, Y. Ishikawa and S. Sato, *Bull. Chem. Soc. Jpn.*, 1980, **53**, 3159-3164.
16. L. G. Piper, M. E. Donahue and W. T. Rawlins, *J. Phys. Chem.*, 1987, **91**, 3883-3888.

17. H. Umemoto, N. Hachiya, E. Matsunaga, A. Suda and M. Kawasaki, *Chem. Phys. Lett.*, 1998, **296**, 203-207.

18. G. Black, T. G. Slanger, G. A. St John and R. A. Young, *J. Chem. Phys.*, 1969, **51**, 116-121.

19. C. Lin and F. Kaufman, *J. Chem. Phys.*, 1971, **55**, 3760-3770.

20. J. T. Herron, *J. Phys. Chem. Ref. Data*, 1999, **28**, 1453-1483.

21. A. Bergeat, K. M. Hickson, N. Daugey, P. Caubet and M. Costes, *Phys. Chem. Chem. Phys.*, 2009, **11**, 8149-8155.

22. M. Gonzalez, R. Valero and R. Sayos, *J. Chem. Phys.*, 2000, **113**, 10983-10998.

23. J. Li, P. Caridade and A. J. C. Varandas, *J. Phys. Chem. A*, 2014, **118**, 1277-1286.

24. J. Li and A. J. C. Varandas, *J. Phys. Chem. A*, 2012, **116**, 4646-4656.

25. B. R. Rowe, G. Dupeyrat, J. B. Marquette and P. Gaucherel, *J. Chem. Phys.*, 1984, **80**, 4915-4921.

26. N. Daugey, P. Caubet, B. Retail, M. Costes, A. Bergeat and G. Dorthe, *Phys. Chem. Chem. Phys.*, 2005, **7**, 2921-2927.

27. N. Daugey, P. Caubet, A. Bergeat, M. Costes and K. M. Hickson, *Phys. Chem. Chem. Phys.*, 2008, **10**, 729-737.

28. R. J. Shannon, C. Cossou, J.-C. Loison, P. Caubet, N. Balucani, P. W. Seakins, V. Wakelam and K. M. Hickson, *RSC Adv.*, 2014, **4**, 26342.

29. R. Grondin, J.-C. Loison and K. M. Hickson, *J. Phys. Chem. A*, 2016, **120**, 4838-4844.

30. K. M. Hickson, J.-C. Loison, H. Guo and Y. V. Suleimanov, *J. Phys. Chem. Lett.*, 2015, **6**, 4194-4199.

31. K. M. Hickson, J.-C. Loison, D. Nuñez-Reyes and R. Méreau, *J. Phys. Chem. Lett.*, 2016, **7**, 3641-3646.

32. T. Suzuki, Y. Shihira, T. Sato, H. Umemoto and S. Tsunashima, *J. Chem. Soc., Faraday Trans*, 1993, **89**, 995-999.

33. A. Bergeat, T. Calvo, G. Dorthe and J.-C. Loison, *Chem. Phys. Lett.*, 1999, **308**, 7-12.

34. D. Chastaing, S. D. Le Picard and I. R. Sims, *J. Chem. Phys.*, 2000, **112**, 8466-8469.

35. S. Andersson, N. Markovic and G. Nyman, *J. Phys. Chem. A*, 2003, **107**, 5439-5447.

36. C. L. Sam and J. T. Yardley, *Chem. Phys. Lett.*, 1979, **61**, 509-512.

37. D. Nuñez-Reyes and K. M. Hickson, *Chem. Phys. Lett.*, 2017, **687**, 330-335.

38. S. P. Sander, J. Abbatt, J. R. Barker, J. B. Burkholder, R. R. Friedl, D. M. Golden, R. E. Huie, C. E. Kolb, M. J. Kurylo, G. K. Moortgat, V. L. Orkin and P. H. Wine, *JPL Publication 10-6, Jet Propulsion Laboratory, Pasadena, 2011* http://jpldataeval.jpl.nasa.gov/., 2011.

39. I. R. Sims and I. W. M. Smith, *J. Chem. Soc., Faraday Trans. II*, 1988, **84**, 527-539.

40. R. J. Donovan and D. Husain, *Chem. Rev.*, 1970, **70**, 489-516.